Control Surface Fault Diagnosis with Specified Detection Probability - Real Event Experiences

Hansen, Søren; Blanke, Mogens

Published in:
Proceedings of the 2013 International Conference on Unmanned Aircraft Systems

Link to article, DOI:
10.1109/ICUAS.2013.6564729

Publication date:
2013

Control Surface Fault Diagnosis with Specified Detection Probability - Real Event Experiences

Søren Hansen[1] and Mogens Blanke[2]

Abstract— **Diagnosis of actuator faults is crucial for aircraft since loss of actuation can have catastrophic consequences. For autonomous aircraft the steps necessary to achieve fault tolerance is limited when only basic and non-redundant sensor and actuators suites are present. Through diagnosis that exploits analytical redundancies it is, nevertheless, possible to cheaply enhance the level of safety. This paper presents a method for diagnosing control surface faults by using basic sensors and hardware available on an autonomous aircraft. The capability of fault diagnosis is demonstrated obtaining desired levels of false alarms and detection probabilities. Self-tuning residual generators are employed for diagnosis and are combined with statistical change detection to form a setup for robust fault diagnosis. On-line estimation of test statistics is used to obtain a detection threshold and a desired false alarm probability. A data based method is used to determine the validity of the methods proposed. Verification is achieved using real data and shows that the presented diagnosis method is efficient and could have avoided incidents where faults led to loss of aircraft.**

I. INTRODUCTION

One of the main challenges when dealing with autonomous aircraft is diagnosis and handling of faults in sensors and actuators. Loss or partly loss of actuation is particularly critical for the aircraft. Since price and weight are important competition parameters for unmanned aerial vehicles (UAVs), cheap materials and solutions are sometimes used, which increase the risk of faults. Diagnosis of such faults can enhance the safety and usability of UAVs and thereby increase their value both in terms of economy but more importantly in terms of safety.

The subject of fault diagnosis (FDI) and fault tolerant control (FTC) for general aircraft is a huge field of interest in academia as well as in industry. A recent survey [1] analyzed different approaches to FDI and FTC where methods using observer-based design, on-line recursive parameter estimation, sliding mode control with control allocation and predictive control were all investigated. Recent FDI work for general aircraft also include [2] and [3] where model based approaches were treated and [4] where the methods used by Airbus were explained. A general structural analysis were conducted in [5] for a non-linear aircraft model, and structural detectability and isolability properties were determined.

Loss of control surfaces was the topic of [6] and [7] where a flight controller robust towards partial loss of flaps was designed for a general aircraft. Oscillations in control surfaces for large passenger aircraft were investigated in [8] that also covered performance monitoring of the surfaces.

Extensive research has been conducted for UAVs related to control surface faults. These include [9] and [10] where the focus was on how faults directly affect the UAV's ability to maneuver. Reconfigurations of the control and guidance systems were done to accommodate the reduced capabilities of the aircraft. The FDI was achieved by using an extended version of multiple model adaptive estimation (MMAE) first reported in [11]. The faults were modelled as an unknown signal controlling the actuators, which were then estimated by extended Kalman filters in the enhanced MMAE method. In [12] FTC for a small UAV subject to control surface faults was investigated. The authors estimated the reduction of UAV's flight envelope and used active FDI to isolate faults on the control surfaces. Methods using linear parameter varying methods were dealt with in [13]. The problem of probability of timely diagnosis and recovery was dealt with in [14].

The subject of this paper is also FDI for control surfaces of a small UAV. A low-order model between the aircraft control surface deflections and the measured angular rates is estimated online and utilized to create a set of residual signals. These signals indicate faults and are used directly for the detection. Statistical methods are used to accept or reject hypothesis about the UAV's condition. A salient feature is shown to be that self-tuning is possible during a flight. In the paper, this is demonstrated using real data from both normal and faulty flights. Although only a few cases of actual faults were recorded, this will be shown to allow us to investigate the performance in diagnostic terms of detection and false alarm probabilities from real data.

The paper is organized as follows. Introduction and a brief description of the UAV used in the tests is followed by, a general FDI setup with parameter adaptation in residual generators, where-after model structure and adaptation algorithm are elaborated. A statistical framework leading to a hypothesis test is then introduced and performance of the system is discussed based on processing of real data. A conclusion summarizes the paper.

II. TEST AIRCRAFT

The aircraft considered in this paper is a Banshee target drone build by Meggitt Defence System [15] (Fig. 1). The drone is a delta wing aircraft equipped with a small rear mounted Wankel engine which gives thrust through a 2 bladed wooden propeller. It is launched from a catapult system and lands by parachute. The aircraft is equipped with

[1]S. Hansen is with DTU Electrical Engineering, Technical University of Denmark, Elektrovej B. 326, DK-2800 Lyngby, Denmark. (sh@elektro.dtu.dk).

[2]M. Blanke is with DTU Electrical Engineering, Technical University of Denmark, Elektrovej B. 326, DK-2800 Lyngby, Denmark and AMOS Centre of Excellence, Norwegian University of Science and Technology, NTNU, NO-7491 Trondheim, Norway. (mb@elektro.dtu.dk).

a basic autopilot system and is operated from ground by an operator. The aircraft can be flown by remote control but this is only done rarely. During normal missions the aircraft is flown by its autopilot and the operator merely gives waypoints that it should follow.

The aircraft is equipped with only two actuators, in addition to an engine throttle δ_t, which is not considered in this paper. The actuators are ailerons δ_a and elevators δ_e. Both are placed side by side on the delta wing. The aircraft has a fixed tail without rudder. The pair of ailerons are locked together in software such that actuation of one flap is not possible without also moving the other. In the remaining part of the paper the ailerons are treated as one actuator and the same applies to the elevators. None of the flaps has angle measurement attached, with the consequence that the autopilot is vulnerable to stuck or disconnected surfaces.

Fig. 1. Banshee drone at a Danish Defense exercise. *Foto: VFD*

The Banshee is equipped with a barometric sensor which measures the flying height, h and a pitot tube to measure the airspeed, v_a. The onboard Inertial Measurement Unit (IMU) estimates the attitude of the aircraft $\mathbf{\Phi} = \begin{bmatrix}\phi & \theta & \psi\end{bmatrix}^{\mathrm{T}}$. This is done based on measurements from inertial navigation sensors such as the three-axis gyro measuring the aircraft turn rates $\boldsymbol{\omega} = \begin{bmatrix}p & q & r\end{bmatrix}^{\mathrm{T}}$. Apart from these a standard GPS is onboard to get the position of the aircraft and correct the attitude estimate.

Telemetry data is send to a ground station over a radio link. This is the data used for the FDI. Due to the limited bandwidth of the radio link, sensor values are not available at full rate. This entail that faster dynamics are lost and this issue need be considered when designing the FDI system.

III. FAULT DIAGNOSIS MODEL

The FDI setup used in this paper is illustrated in Fig. 2. The general idea is to use a model that is adapted, online, to the smaller variations in aircraft and external conditions. The output of this model is compared to the measurements of the aircraft to form a residual signal. The adaptation is achieved by feeding back the residual signals and change model parameters to give a better fit in next iteration. The residual signal is also monitored by a change detection

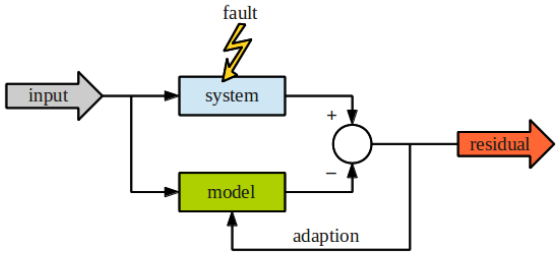

Fig. 2. Adaptive fault detection setup.

system, which stops the adaptation if a too abrupt change happens. This would indicate that a fault has occurred on the aircraft. By stopping the adaptation it is avoided to adapt the model to a faulty state of the system.

The FDI setup is developed as an aid to the UAV operator and is therefore not integrated in the autopilot hardware even though this could easily be done. This means all processing is done on telemetry signals send from the aircraft to the ground station. The limited sample-rate available from the telemetry entails that the chosen model does not need to include fast dynamics as these will not be identifiable anyway. Since the operator must act on the alarm signals coming from FDI system it is important to investigate if the system is able to raise alarms fast enough to give the operator sufficient reaction time before the aircraft is lost.

IV. CONTROL SURFACE FAULT MODEL

An aircraft can be described by a 6 degree of freedom model including kinematic and dynamic equations (see eg. [16]). Utilizing this model implies detailed knowledge about the aerodynamic coefficients and this information is not always available for cheaper UAV's. For control surface fault diagnosis the important feature is the relationship between surface deflection and angular rates. In this paper an adaptive model of this relationship is employed. The following three relations for roll rate (p), pitch rate (q) and yaw rate (r), calculated at sample k, is related to the aileron deflection δ_a and elevator deflection δ_e.

$$p[k] = a_{pa}\delta_a[k] + b_{pa} \quad (1)$$

$$q[k] = a_{qe}\delta_e[k] + b_{qe} \quad (2)$$

$$r[k] = a_{ra}\delta_a[k] + b_{ra}r[k-1] + c_{ra} \quad (3)$$

where b_{pa}, b_{qe} and c_{ra} are bias terms and a_{pa}, a_{qe} and a_{ra} are gain factors. Equation (3) includes the integrating effect between the aileron and yaw rate in the b_{ra} term. This approach separates the lateral and longitudinal states since the aileron is only related to roll and yaw and the elevator is related to pitch.

Equations (1) to (3) can be described on the form

$$y[k] = \boldsymbol{\varphi}[k]^{\mathrm{T}}\boldsymbol{\Theta}[k] + e[k] \quad (4)$$

TABLE I

FAULT DEPENDENCIES OF RESIDUALS

	p	q	r	δ_a	δ_e
R_{pa}	1	0	0	1	0
R_{qe}	0	1	0	0	1
R_{ra}	0	0	1	1	0

with $e[k]$ being the unmodelled behavior. For (1) the parameters would be:

$$y[k] = p[k] \quad (5)$$

$$\boldsymbol{\varphi}[k] = \begin{bmatrix} \delta_a[k] \\ 1 \end{bmatrix} \quad (6)$$

$$\boldsymbol{\Theta}[k] = \begin{bmatrix} a_{pa} \\ b_{pa} \end{bmatrix} \quad (7)$$

From the general expression given by (4) residuals are,

$$\varepsilon[k] = y[k] - \boldsymbol{\varphi}[k]^{\mathrm{T}}\boldsymbol{\Theta}[k] \quad (8)$$

Control surface defects will give rise to rapid change in the input/output signals and hence in the prediction error (8) and subsequently appear as a parameter adaptation to the faulty case.

Three residuals are formed based on (8): R_{pa} from (1), R_{qe} from (2) and R_{ra} from (3).

$$R_{pa} = p[k] - a_{pa}\delta_a[k] - b_{pa} \quad (9)$$

$$R_{qe} = q[k] - a_{qe}\delta_e[k] - b_{qe} \quad (10)$$

$$R_{ra} = r[k] - a_{ra}\delta_a[k] - b_{ra}r[k-1] - c_{ra} \quad (11)$$

This gives rise to a binary dependency between residuals and actuator faults as shown in Table I. To truly isolate a fault the column-wise signature of each variable must be unique. As seen from the table both q and the elevator deflection δ_e has the column signature $[0,1,0]$. This means that if residual R_{qe} indicates a fault but R_{pa} and R_{ra} does not, it is not possible to isolate whether the fault is caused by the sensor for q or the elevator. Active fault diagnosis methods are useful to isolate this type of fault. However since practical experience with this particular drone shows that flap faults are much more likely to occur than single faults on gyros, a single indication on R_{qe} is interpreted as an elevator fault.

A. Online parameter estimation

The a, b and c parameters of the residuals (9)-(11) are estimated online using recursive least squares (RLS),

$$\varepsilon[k] = y[k] - \boldsymbol{\varphi}[k]^{\mathrm{T}}\hat{\boldsymbol{\Theta}}[k-1] \quad (12)$$

$$P[k] = \left(\lambda_f P[k-1]^{-1} + \boldsymbol{\varphi}[k]\boldsymbol{\varphi}[k]^{\mathrm{T}}\right)^{-1} \quad (13)$$

$$\hat{\boldsymbol{\Theta}}[k] = \hat{\boldsymbol{\Theta}}[k-1] + P[k]\boldsymbol{\varphi}[k]\boldsymbol{\varepsilon}[k] \quad (14)$$

In this, λ_f is the forgetting factor and $P[k]$ is the estimators covariance. The initial value of $P[k]$ is found empirically from several test flights. This is done by running the estimator for data from steady wings-level flight and see what value of $P[k]$ settles at. The forgetting factor is tuned such that past measurements does not influence the estimate too much. This is done to decrease the risk of raising false alarms

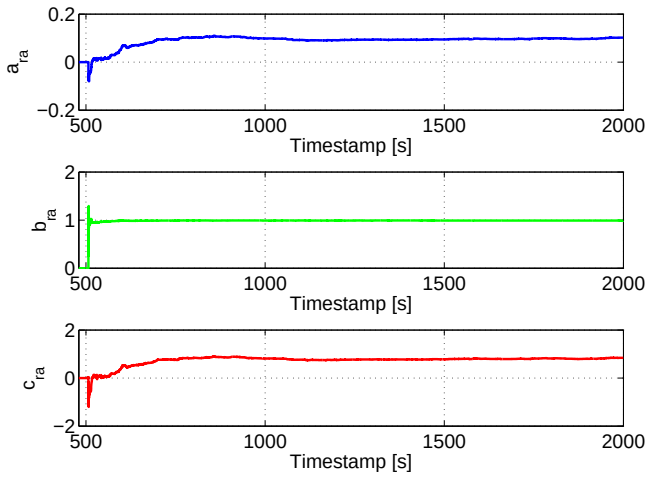

Fig. 3. Parameter estimates for R_{ra}. The estimation is started just after 500 s.

because of small unmodelled disturbances. Fig. 3 shows how the parameters of the estimator for (11) develop over time. The parameters are in this case initialized at 0 to see how quickly they converges to a steady value. For a_{ra} and c_{ra} it takes around 200 s to settle. To reduce the initial transient, parameters are initialized with their expected normal values.

B. Residual whitening

By analyzing the residuals power spectrum density and autocorrelation functions it is found that a heavy correlation is present on the signals. This is illustrated for R_{pa} in the leftmost two plots of Fig. 4. The correlation is due to the low-order model used when generating the residuals. In order

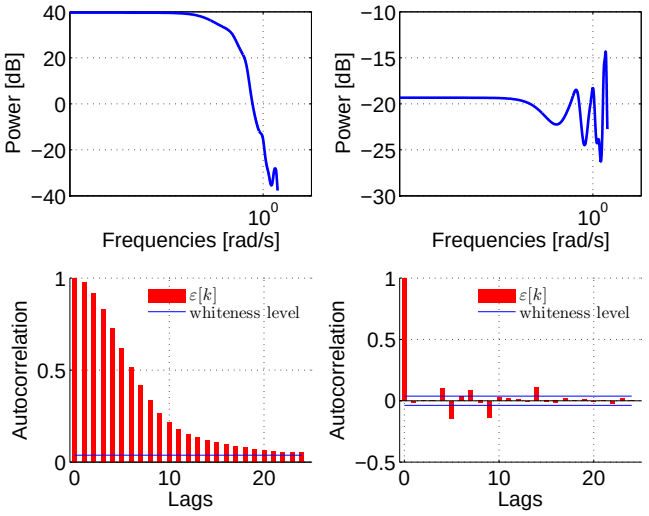

Fig. 4. Power spectrum density and autocorrelation of residual (9) before and after whitening.

not to degrade the performance of the change detector by this correlation the signals are run through a whitening filter before further processing. A finite impulse response (FIR) representation of a linear estimator can be used to estimate

the deterministic part of the signal

$$\hat{\varepsilon}[k] = \sum_{j=1}^{J} a_j \varepsilon[k-j] \tag{15}$$

By subtracting the estimate $\hat{\varepsilon}[k]$ from the actual signal only the stochastic part will be left.

$$\tilde{\varepsilon}[k] = \varepsilon[k] - \hat{\varepsilon}[k] \tag{16}$$

In practice, a size of $J = 5$ in (15) was found sufficient and the coefficients a_j were found by optimization over a representative data-set of each residual. This was done once. In the right plots of Fig. 4 the autocorrelation is shown after whitening. Although the signal is not perfectly white this is found to be satisfactory for the change detection.

C. Distribution of Residuals

The residual signals given in Table I is found to follow the Laplacian distribution which have the following density function

$$p(x;a,b) = \frac{1}{2b}\exp\left(-\frac{|x-a|}{b}\right) \tag{17}$$

where a is the median and b is the scaling. By running a Kolmogorov-Smirnov test on the data it is verified that they follow the Laplacian distribution. This is done for a sample of consecutive residual data which are tested against a distribution where a and b in (17) are substituted by their maximum likelihood estimates (MLEs). The result is that with a p-value of 0.064 the data come from the same distribution. A similar test is done for the MLE Gaussian distribution but with a p-value of only 4.5×10^{-4}, data cold not be Gaussian. Both tests were done on the data after the whitening process.

V. HYPOTHESIS TEST

Changes in the three residual signals are detected using the Generalized Likelihood Ratio Test (GLRT). The GLRT distinguishes between two different hypothesis about the parameters, $\boldsymbol{\Theta}$, of the involved probability distribution. In this case $\boldsymbol{\Theta} = a$ in (17).

The nominal case, $\mathscr{H}_0$, for the residuals is when their median value a is close to zero. A median different from zero indicate a discrepancy between the aircraft model and the measurements which in terms indicate a fault (See eg. Fig. 2). The two hypothesis for fault detection are therefore

$$\mathscr{H}_0 : a = 0 \tag{18}$$

$$\mathscr{H}_1 : a \neq 0 \tag{19}$$

The scaling parameter, b, is not known for either case and is therefore to be estimated.

A. GLR test for Laplacian

A test statistic for the Laplacian distribution for changes to the median a, can be formulated by the following expression

$$T_L'(\boldsymbol{x}) = \left(\frac{\hat{b}_0}{\hat{b}_1}\right)^N > \gamma' \tag{20}$$

TABLE II

GLRT PARAMETERS FOR RESIDUALS.

	Window size (N)	Threshold (γ)
R_{pa}	100	100
R_{qe}	100	100
R_{ra}	75	50

with the MLE's of the parameters given by

$$\hat{b}_0 = \frac{1}{N}\sum_{n=1}^{N} |x[n]| \tag{21}$$

$$\hat{b}_1 = \frac{1}{N}\sum_{n=1}^{N} |x[n] - \text{median}(\boldsymbol{x})| \tag{22}$$

When the value of $T_L'(\boldsymbol{x})$ is larger than the threshold value γ' the $\mathscr{H}_0$ hypothesis is rejected and data indicate a median significantly apart from 0.

To achieve an expression that is more suitable for practical calculations and does not have numerical issues the following conversion of (20) is done.

$$T_L(\boldsymbol{x}) = N\log\left(\frac{\hat{b}_0}{\hat{b}_1}\right) > \gamma \tag{23}$$

The threshold value γ should be chosen appropriately and a data based method for doing this is given in the next section. See eg. [17] for a details of the general GLRT.

VI. DETECTOR PERFORMANCE

The parameters for the detectors working on the three residual signals are given in Table II.

The window size N is chosen such that a suitable batch of data is treated in each recursion. The threshold is chosen based on a statistical analysis of values from the GLRT output, an approach first presented by [18] and applied in airspeed sensor fault diagnosis for UAVs in [19]. Fig. 5 shows a probability plot of this output for two different flights. The plotted time-history is from residual R_{ra}, the other residuals have a similar appearance. The output follows approximately a Weibull distribution with the following distribution function,

$$P(x;b_w,k_w) = 1 - \exp\left(-\left(\frac{x}{b_w}\right)^{k_w}\right) \tag{24}$$

It is possible to estimate the scale parameter b_w and shape parameter k_w by eg. MLE methods. By using the right-tail probability $Q(x;b_w,k_w) = 1 - P(x;b_w,k_w)$ a measure of the probability of false alarms P_{FA} for certain thresholds is given. For $\gamma = 50$ a probability of $P(x;b_w,k_w) = 0.9999$ is achieved. This means that statistically 0.9999 of $\mathscr{H}_0$ data will be located below the threshold which entail a $P_{FA} = 0.0001$. The residuals R_{pa} and R_{qe} is more noisy and therefore higher values of γ are found for them.

By using data from an incident related to aileron malfunction it is possible to analyze performance of the change detection system. Fig. 6 shows roll and pitch angles together with commanded aileron deflection. The first observation

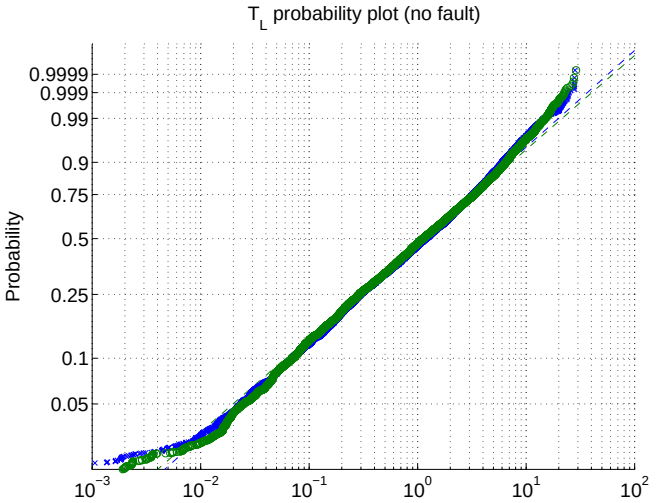

Fig. 5. Probability plot of the test statistic output T_L when the aircraft is fault free.

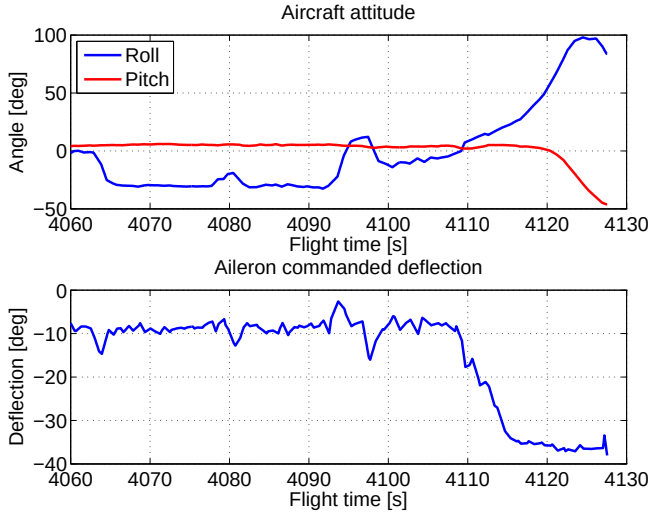

Fig. 6. Selected telemetry records from aircraft just before crash.

is that much of the dynamics of the aileron signal is lost due to the low sample-rate of the telemetry data. Secondly just before $t = 4110$ s the aircraft starts rolling right, even though the autopilot commands a left roll. From this point on there is no relation between the commanded signal and the aircraft's maneuvers. This clearly shows that the relations of (9) is violated. The aircraft crashes shortly after and the subsequent investigation of the crash determined that control of an aileron was lost in flight.

To give an assessment of the diagnosis systems ability to detect faults with the data chosen threshold value, analysis of data belonging to the $\mathscr{H}_1$ case is done. Since the starting point of a $\mathscr{H}_1$ condition is not known exact there is some uncertainty in the following analysis. However it gives a fair estimate of the actual detection probability, P_D, under real-life conditions. Fig. 7 shows T_L for R_{ra} for two different cases where faults occurs on the ailerons of a Banshee. The top plot is from a case where the linkage mechanism, which

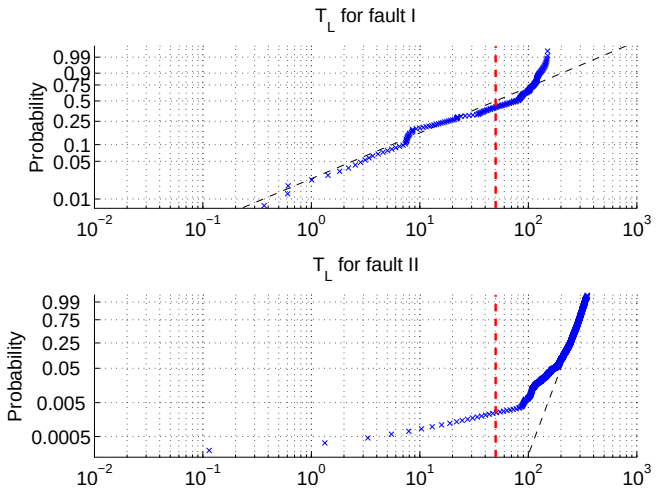

Fig. 7. Probability plot of the test statistic output T_L for two different fault cases. The vertical dashed line indicates the detector threshold.

drives one of the flaps, slips in its gears causing an actuator offset. This does not trigger a crash in this particular case but could lead reduced maneuverability since the deflection to one side is decreased. The P_D for this case is 58%. The bottom plot of Fig. 7 is the case of total loss of aileron actuation illustrated in Fig. 6 that within shortly caused a crash of the aircraft. This case has a P_D of 98%.

Fig. 8 shows normalized histograms for R_{pa} for two segments of flight. The nominal segment is centered around 0 as expected, and the faulty segment shows an shift in median. The Laplacian shape of the $\mathscr{H}_1$ data are slightly

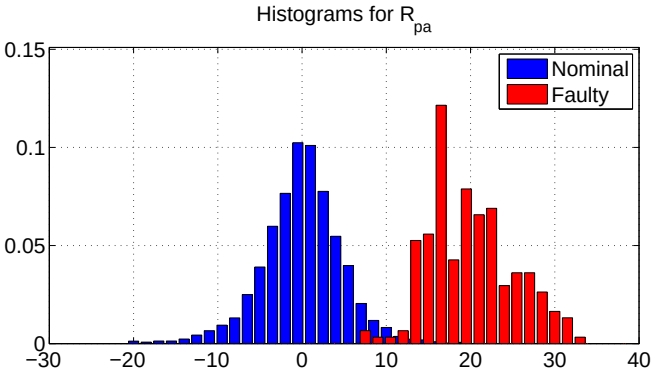

Fig. 8. Histogram for a segment of R_{pa} of normal flight shown together with a faulty segment. The switch in median value is apparent.

blurred because the fault does not affect the residual in a sharp step but rather in a softer fashion. The hypothesis test can, anyway, be done over a window size of 100 samples.

Fig. 9 depicts the time development for the three residuals (9)-(11) for this flight. There is an indication of a change in center value at the end of the plots.

Fig. 10 shows the test statistics for the three residuals (9)-(11), In this figure the fault indication at around $t = 4100$ s is more significant than on Fig. 9. The fault is detected $12-14$ s before control of the aircraft is lost at $t = 4116$ s. This fault signal could give the UAV operator enough time

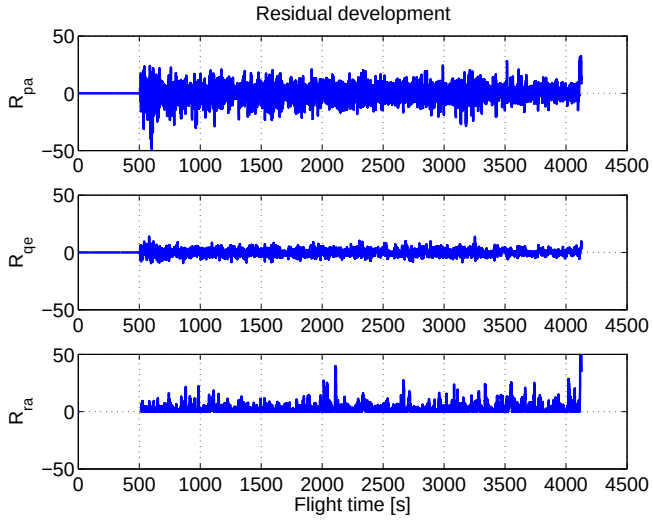

Fig. 9. Development over time for the three residuals for a flight with an aileron fault.

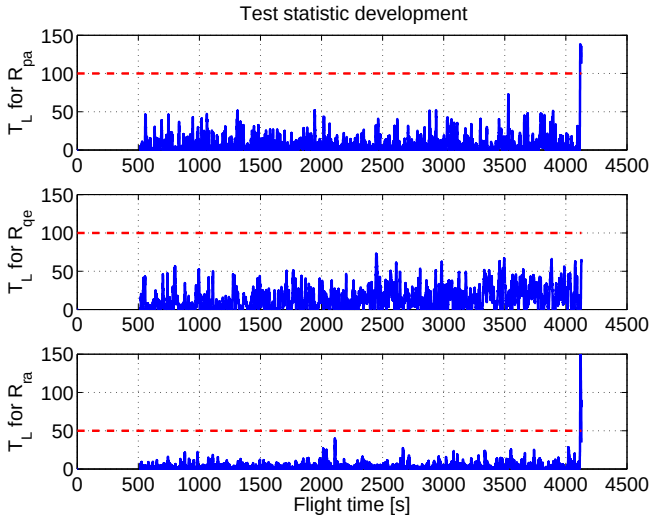

Fig. 10. Development over time for the three test statistics for a flight with an aileron fault.

to react and deploy the parachute in order to bring down the aircraft in a controlled manner, but a automatic fail-safe mechanism integrated in the UAV's autopilot could have saved the aircraft.

VII. CONCLUSIONS

This paper investigated change detection methods used for detection of control surface faults for UAVs. The suggested method utilized that the control surfaces have direct influence on the aircraft angular rates. A number of low-order models relating these rates to the actuator deflections were presented and by utilizing parameter estimation small disturbances could be overcome. Results with real-life data assessed the need for whitening filters before the GLRT change detection methods could be used. The thresholds for the test statics were found by analyzing segments of real-life data. The suggested method does not require a large amount on computational power and is therefore well suited for implementation in an existing autopilot system.

ACKNOWLEDGMENT

The Danish Forces Joint Drone Team is gratefully acknowledged for their help in collecting flight data and conducting experiments and for providing research funding.

REFERENCES

[1] C. Edwards, T. J. J. Lombaerts, and M. H. Smaili, Eds., *Fault Tolerant Flight Control: A Benchmark Challenge*. Springer, 2010.
[2] A. Zolghadri, "Advanced model-based fdir techniques for aerospace systems: Today challenges and opportunities," *Progress in Aerospace Sciences*, vol. 53, pp. 18–29, 2012.
[3] J. Marzat, H. Piet-Lahanier, F. Damongeot, and E. Walter, "Model-based fault diagnosis for aerospace systems: a survey," *Journal of Aerospace Engineering*, vol. 226, no. 10, pp. 1329–1360, 2012.
[4] P. Goupil, "Airbus state of the art and practices on fdi and ftc in flight control system," *Control Engineering Practice*, vol. 19 (6), pp. 524 – 539, 2011.
[5] M. L. Fravolini, V. Brunori, G. Campa, M. R. Napolitano, and M. La Cava, "Structured analysis approach for the generation of structured residuals for aircraft fdi," *IEEE Transactions on Aerospace and Electronic Systems*, vol. 45 (4), pp. 1466–1482, 2009.
[6] X. Yu and J. Jiang, "Fault-tolerant flight control system design against control surface impairments," *IEEE Aerospace and Electronics Systems*, vol. 20 (4), pp. 871–886, 2012.
[7] ——, "Hybrid fault-tolerant flight control system design against partial actuator failures," *IEEE Transactions on Control Systems Technology*, vol. 20 (4), pp. 872–876, 2012.
[8] E. Alcorta-Garcia, A. Zolghadri, and P. Goupil, "A nonlinear observer-based strategy for aircraft oscillatory failure detection: A380 case study," *IEEE Transactions on Aerospace And Electronic Systems*, vol. 47 (4), pp. 2792–2806, 2011.
[9] G. Ducard and H. P. Geering, "Efficient nonlinear actuator fault detection and isolation system for unmanned aerial vehicles," *Journal of Guidance, Control, and Dynamics*, vol. 31 (1), pp. 225–237, 2008.
[10] G. J. J. Ducard, *Fault-tolerant Flight Control and Guidance Systems*. Springer Verlag, 2009.
[11] D. Magill, "Optimal adaptive estimation of sampled stochastic processes," *Automatic Control, IEEE Transactions on*, vol. 10, pp. 434–439, 1965.
[12] F. Bateman, H. Noura, and M. Ouladsine, "Fault diagnosis and fault-tolerant control strategy for the aerosonde uav," *IEEE Transactions on Aerospace and Electronic Systems*, vol. 47, no. 3, pp. 2119–2137, 2011.
[13] D. Henry, A. Zolghadri, J. Cieslak, and D. V. Efimov, "A lpv approach for early fault detection in aircraft control surfaces servo-loops," in *Proc. 8th IFAC Symp. on Fault Detection, Supervision and Safety of Terchnical Processes, SAFEPROCESS 2012*, Mexico, 2012, pp. 806 – 811.
[14] N. E. Wu, "Coverage in fault-tolerant control," *Automatica*, vol. 40, no. 4, pp. 537 – 548, 2004.
[15] Meggitt Defence Systems Ltd., "Meggitt defence systems uk," 2012. [Online]. Available: http://www.meggittdefenceuk.com/
[16] B. L. Stevens and F. L. Lewis, *Aircraft Control and Simulation*, 2nd ed. John Wiley & Sons, 2003.
[17] S. M. Kay, *Fundamentals of Statistical Signal Processing: Detection Theory*. Prentice-Hall PTR, 1998.
[18] R. Galeazzi, M. Blanke, and N. K. Poulsen, "Early detection of parametric roll resonance on container ships," *IEEE Transactions on Control Systems Technology*, vol. 21 (2), pp. 489–503, 2013.
[19] S. Hansen and M. Blanke, "Diagnosis of airspeed measurement faults for unmanned aerial vehicles," *IEEE Trans. Aerospace and Electronic Systems (TAES)*, 2013, in print.